A programmable Fresnel transform pulse shaper

G. Mínguez-Vega[1], J.D. McKinney[2] and A.M. Weiner[2]

[1]*Departament de Ciencies Experimentals, Universitat Jaume I, 12080 Castelló, Spain*
[2]*Purdue University, School of Electrical and Computer Engineering*
465 Northwestern Avenue, West Lafayette, IN 47907-2035
mckinnjd@purdue.edu

Abstract: We demonstrate the first reprogrammable Fresnel transform pulse shaper based on a modified direct space-to-time pulse shaping apparatus. In our approach, the pulse shaping lens and mask are implemented by a dual-layer liquid crystal spatial light modulator. The input mask subsequently undergoes a free-space Fresnel transform which causes quadratic dispersion of the output temporal waveform. When used as a spectrometer, we demonstrate that the passband function of the apparatus (determined by the Fourier transform of the input spatial mask) may be chosen to exhibit a user-defined scale. Here we present the theory of operation, as well as experimental verification in both the time- and frequency-domains.

OCIS codes: (320.5540) Pulse shaping; (320.1590) Chirping; (260.2030) Dispersion

References and links

1. A. M. Weiner, "Femtosecond pulse shaping using spatial light modulators," Rev. Sci. Instrum. **71**, 1929–1960 (2000).
2. A. M. Weiner, "High-resolution femtosecond pulse shaping," J. Opt. Soc. Am. B **5**, 1563–1572 (1988).
3. Y. T. Mazurenko, "Holography of wave packets," Appl. Phys. B **50**, 101–114 (1990).
4. A. M. Weiner, D. E. Leaird, D. H. Reitze, and E. G. Paek, "Femtosecond spectral holography," IEEE J. Quantum Electron. **28**, 2251–2261 (1992).
5. M. C. Nuss, M. Li, T. H. Chiu, A. M. Weiner, and A. Partovi, "Time-to-space mapping of femtosecond pulses," Opt. Lett. **19**, 664–666 (1994).
6. P. C. Sun, Y. T. Mazurenko, W. C. S. Chang, P. K. L. Yu, and Y. Fainman, "All optical parallel-to-serial conversion by holographic spatial-to-temporal frequency encoding," Opt. Lett. **20**, 1728–1730 (1995).
7. M. C. Nuss and R. L. Morrison, "Time-domain images," Opt. Lett. **20**, 740–742 (1995).
8. D. E. Leaird and A. M. Weiner, "Femtosecond direct space-to-time pulse shaping," IEEE J. Quantum Electron. **37**, 494–504 (2001).
9. D. E. Leaird and A. M. Weiner, "Femtosecond optical packet generation by a direct space-to-time pulse shaper," Opt. Lett. **24**, 853–855 (1999).
10. C. Froehly, B. Colombeau, and M. Vampouille, "Shaping and analysis of picosecond light pulses," in *Prog. Opt. XX*, E. Wolf, ed., pp. 65–153 (Elsevier, Amsterdam, 1983).
11. D. E. Leaird and A. M. Weiner, "Chirp control in the direct space-to-time pulse shaper," Opt. Lett. **25**, 850–852 (2000).
12. J. D. McKinney, D. S. Seo, and A. M. Weiner, "Direct Space-to-Time Pulse Shaping at 1.5 μm," IEEE J. Quantum Electron. **39**, 1635–1644 (2003).
13. D. E. Leaird and A. M. Weiner, "Femtosecond direct space-to-time shaping in an integrated optical configuration," Opt. Lett. **29**, 1551–1553 (2004).
14. M. M. Wefers and K. A. Nelson, "Generation of high-fidelity programmable ultrafast optical waveforms," Opt. Lett. **20**, 1047–1049 (1995).
15. A. M. Weiner, D. E. Leaird, J. S. Patel, and J. R. Wullert, "Programmable femtosecond pulse shaping by use of a multielement liquid-crystal phase modulator," Opt. Lett. **15**, 326–328 (1990).

#8348 - $15.00 USD Received 4 August 2005; revised 20 September 2005; accepted 21 September 2005

16. A. M. Weiner, D. E. Leaird, J. S. Patel, and J. R. Wullert, "Programmable shaping of femtosecond optical pulses by use of a 128-element liquid crystal phase modulator," IEEE J. Quantum Electron. **28**, 908–920 (1992).
17. T. Feurer, J. C. Vaughan, R. M. Koehl, and K. A. Nelson, "Multidimensional control of femtosecond pulses by use of a programmable liquid-crystal matrix," Opt. Lett. **27**, 652–654 (2002).
18. J. D. McKinney and A. M. Weiner, "Engineering of the Passband Function of a Generalized Spectrometer," Opt. Express **12**, 5022–5036 (2004), http://www.opticsexpress.org/abstract.cfm?URI=OPEX-12-21-5022.
19. M. B. Sinclair, M. A. Butler, S. H. Kravitz, W. J. Zubrzycki, and A. J. Ricco, "Synthetic Infrared Spectra," Opt. Lett. **22**, 1036–1038 (1997).
20. O. E. Martinez, "Grating and prism compressors in the case of finite beam size," J. Opt. Soc. Am. B **3**, 929–934 (1986).
21. A. E. Siegman, *Lasers* (University Science Books, Sausalito, 1986).
22. A. Papoulis, "Pulse Compression, Fiber Communications, and Diffraction: A Unified Approach," J. Opt. Soc. Am. A **11**, 3–13 (1994).
23. C. Palma and V. Bagini, "Extension of the Fresnel transform to ABCD systems," J. Opt. Soc. Am. A **14**, 1774–1779 (1997).
24. J. Lancis, G. Mínguez-Vega, E. Tajahuerce, V. Climent, P. Andrés, and J. Caraquitena, "Chromatic compensation of broadband light diffraction: ABCD-matrix approach," J. Opt. Soc. Am. A **21**, 1875–1885 (2004).

1. Introduction

Synthesis of ultrafast arbitrary optical waveforms has attracted much attention over the last several decades due to a huge number of applications in areas such as optical communications, spectroscopy, and nonlinear optics [1]. Synthesis of these waveforms is achieved primarily via two optical pulse shaping geometries in the femtosecond regime: the Fourier transform (FT) and the direct space-to-time (DST) pulse shapers. The most common configuration is the FT architecture which allows the creation of temporal output fields with nearly arbitrary shape [2]. Mathematically, the output temporal waveform is determined by the convolution of the short-pulse input pulse with the FT of an amplitude and/or phase mask applied to the optical spectrum. Since the proposal of spectral holography [3], the similarity between spatial and temporal frequency opened the possibility of interchanging information between these two domains in a Fourier-transform pulse shaping geometry [4, 5, 6, 7]. However, despite the power and widespread use of this technique, the method suffers from the complexity of calculating the required Fourier transform to implement the mask. For applications such as optical communication, where high data rates are desired, this complexity limits the overall system throughput. To overcome this limitation, a straightforward relationship between a specific spatial mask and the output temporal waveform is desirable. To this end, the femtosecond DST pulse shaping apparatus was proposed [8]. In this device, the output temporal field is a directly scaled version of the pulse-shaping mask. Thus, optical parallel-to-serial conversion for generation of optical data packets for communication applications is readily achieved [9].

The DST pulse shaper was initially demonstrated by Froehly and coworkers for picosecond pulses [10]. It is based on the difference between the phase and group velocities introduced across the beam profile by elements with angular dispersion. A simple and effective solution is provided by a tailored grating spectroscope. This architecture allows a frequency modulation and optical frequency control of the output pulse by properly selecting the position of the slit [8, 11]. Due to the importance of high-rate optical pulse sequences at communications wavelengths, significant work has been done to adapt the DST pulse shaper to the 1.5 μm communications wavelength band [12]. At this wavelength integrated optical devices are commonly used and, recently, a modified arrayed waveguide grating, where the slab waveguide section has been removed to obtain direct access to the waveguide array, has been proposed as an alignment-free integrated-optical DST [13]. After the pulse shaper, the control over the dispersion of the output waveform is an important issue for subsequent transmission of the signal over optical fiber networks. To this end, we propose a modified DST pulse shaper based on the Fresnel transform. In this apparatus, the output temporal signal is determined by the

#8348 - $15.00 USD Received 4 August 2005; revised 20 September 2005; accepted 21 September 2005

input field convolved with a scaled representation of the Fresnel transform of the mask. The compact setup, based on a converging input beam configuration, is composed of a two-layer liquid crystal spatial light modulator (LC-SLM) [14], a diffraction grating and a slit. The key feature of our apparatus is the removal of the pulse shaping lens in the conventional DST; this feature is enabled by the use of a two-layer LC-SLM which allows us to implement both the quadratic phase corresponding to the lens, as well as the spatial mask, in a single device. We also introduce a free-space propagation between the mask, also implemented in the SLM, and the diffraction grating. These modifications result in three novel features: (1) Introduction of the SLM produces high flexibility for pulse-shape control allowing virtually continuous phase or amplitude adjustment at every pixel and a reprogrammability at the millisecond time scale; (2) It is possible to select the quadratic dispersion of the output waveform just by adjusting the parameters of the system; and (3) When the apparatus is used as a spectrometer, the passband function determined by the Fourier transform of the mask, can be obtained with a user-defined scaling factor.

While programmable FT pulse shapers utilizing liquid-crystal SLMs have been widely adopted [15, 16, 17], this work represents the first demonstration of such a device in a DST pulse shaper. Our novel configuration may open the possibility of pre-compensation of the parabolic-dispersion associated with pulse propagation in fibers by including the proper dispersion in the optical data packets generated in the DST. The ability to scale the passband function of the device (essentially a generalized spectrometer [18]) in the Fourier regime may also open new possibilities in correlation spectroscopy [19].

This paper is organized as follows. In Section 2 a review of the conventional DST pulse shaper is provided, including a heuristic explanation about how to control the dispersion of the output pulse. In order to reduce the longitudinal size of the setup a more compact design based on a converging input beam is proposed in Section 3. The validity of this new proposal is supported by experimental results that show the equivalent of a Fresnel diffraction pattern in the temporal domain. In Section 4 we study the advantages of this novel arrangement in controlling the scaling of the output spectrum and finally, in Section 5 we conclude.

2. Theory of Operation of the Fresnel Transform Pulse Shaper

2.1. A Brief Review of the Conventional DST Pulse Shaper in an $f-f$ Configuration

A schematic representation of the conventional DST pulse shaper is shown in Fig. 1. The grating has a period p, the incident angle of the input beam is θ_i and $s(x)$ is the complex spatial amplitude distribution of the optical field just before the grating, i.e. the input plane of the apparatus. Note, the x coordinate is defined along the transverse dimension of the spatial amplitude distribution $s(x)$ - parallel to the diffraction grating. At the back focal plane of the lens, a thin slit filters the dispersed spectrum. In this configuration the temporal intensity profile of the output beam is proportional to the intensity of the spatial amplitude distribution $s(x)$ just before the grating. To achieve the desired complex spatial amplitude distribution $s(x)$, a physical spatial mask $m(x)$ is used to spatially pattern the input beam prior to the diffraction grating. In the conventional DST pulse shaper, the mask is imaged onto the diffraction grating. As a result, the complex spatial amplitude distribution $s(x)$ is given by a (potentially scaled) replica of the input mask $m(x)$ multiplied by a quadratic spatial phase. In general, the mask may modify the spatial amplitude and/or phase of the input beam. In this work, the term "mask" applies exclusively to various spatial amplitude masks. The results of our analysis are, however, completely general and are thus applicable amplitude and / or phase masks.

In mathematical terms, the system can be understood within the framework of paraxial Fresnel diffraction theory. Detailed descriptions of the apparatus are given in References [8, 12, 18] - here we briefly review the basic functionality of the apparatus. Given a mask $m(x)$ illuminated

#8348 - $15.00 USD Received 4 August 2005; revised 20 September 2005; accepted 21 September 2005

by a narrowband ($\Delta\omega \ll \omega_o$) pulsed laser source, the complex field just prior to the grating may be expressed as the product of the complex spectrum of the laser source $E_{in}(\omega)$ and $s(x)$ - the (potentially) scaled image of the mask $m(x)$,

$$E_g^-(x,\omega) \propto E_{in}(\omega)\, s(x). \tag{1}$$

The introduction of a diffraction grating couples optical and spatial frequencies through angular dispersion, and introduces a spatial scaling (astigmatism) to the incident field. Thus, the complex field immediately after the diffraction grating is [20]

$$E_g^+(x,\omega) \propto E_{in}(\omega)\, s(\alpha x)\, exp[-j\gamma(\omega-\omega_o)x], \tag{2}$$

where the spatial dispersion parameter (γ) and spatial scaling factor (α) are given by

$$\gamma = \frac{\lambda_o}{cp\cos\theta_d}, \quad \frac{\text{ps}}{\text{mm}} \tag{3}$$

$$\alpha = \frac{\cos\theta_i}{\cos\theta_d}. \tag{4}$$

The lens imparts a quadratic phase factor in the spatial domain. When the grating-lens and lens-slit separations are chosen to be equal to the focal length (f) of the pulse shaper lens as shown in Fig. 1, an exact spatial Fourier transformation is achieved at the slit plane. Thus the complex field just prior to the slit is expressed as

$$E_s^-(x,\omega) \propto E_{in}(\omega) \int dx'\, s(\alpha x')\, exp\left\{ j\left[\frac{\omega_o}{cf}x - \gamma(\omega-\omega_o)\right]x'\right\} \tag{5}$$

$$\propto E_{in}(\omega)\, S\left\{\frac{1}{\alpha}\left[\frac{\omega_o}{cf}x - \gamma(\omega-\omega_o)\right]\right\}, \tag{6}$$

where S is the spatial Fourier transform of the complex spatial amplitude distribution $s(x)$ just prior to the diffraction grating. When the field described by Eq. (6) is sampled with an ideal spatial delta-function slit positioned at transverse position x_s in the output plane of the apparatus, the complex field just after the slit is given by

$$E_s^+(x,\omega) \propto E_{in}(\omega)\, S\left\{-\frac{\gamma}{\alpha}[\omega-\omega(x_s)]\right\}, \tag{7}$$

where $\omega(x_s)$ is the center wavelength at the slit location x_s. Performing an inverse Fourier transform with respect to optical frequency, we obtain the temporal output of the apparatus

$$e_{out}(t) \propto e_{in}(t) * s\left(-\frac{\alpha}{\gamma}t\right) \tag{8}$$

as previously described [8]. Here, $*$ stands for convolution and

$$\frac{\gamma}{\alpha} = \frac{\lambda_o}{cp\cos\theta_i} \tag{9}$$

is the space-to-time conversion constant in ps/mm, where c is the speed of light and λ_o is the central wavelength. For a sufficiently short input pulse (or large space-to-time conversion constant) the problem of generating the desired output temporal waveform is equivalent to the task of introducing the proper spatial amplitude distribution over the grating.

In the following subsections we describe how modification of the spatial masking operation, along with tunable control of the lens focal length and position relative to the output slit, affects the temporal output of our apparatus. Specifically, we show how the temporal output may be variably tuned from the Fresnel transform of the input spatial mask to a directly-scaled version of the spatial mask - as in the conventional DST pulse shaper - though with variable temporal scale.

#8348 - $15.00 USD Received 4 August 2005; revised 20 September 2005; accepted 21 September 2005

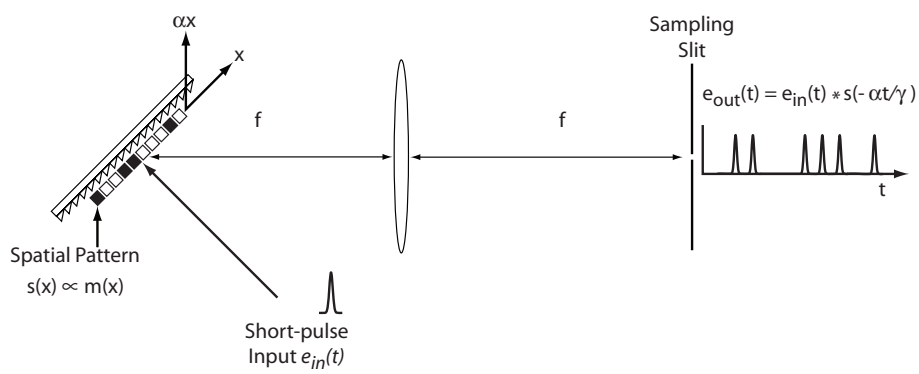

Fig. 1. Sketch of the conventional $f-f$ configuration DST pulse shaper. Here, the spatial amplitude distribution immediately prior to the grating may be a projection of a spatial mask applied to the input beam prior to the DST pulse shaper (for example, via an imaging or telescopic operation).

2.2. *Heuristic explanation of dispersion control in the conventional configuration*

One of the biggest obstacles to the transmission of electromagnetic waves over large distances is material dispersion. Next, we use the well-known duality between paraxial diffraction in space and dispersion in time to propose the introduction of a controlled dispersion in the output waveform of the DST pulse shaper. To this end let us remember that, given an amplitude distribution of a certain mask $m(x)$ illuminated by a plane wave, free space propagation over a distance is a linear shift invariant system whose point spread function is a quadratic spatial phase. Therefore, after free space propagation along a distance R the amplitude distribution is expressed by the following convolution [21]

$$s(x) \;=\; m(x) * exp\left(-i\frac{\pi}{\lambda_o R}x^2\right). \tag{10}$$

Given the mapping from space to time in the apparatus, to obtain a tunable temporal dispersion in the output of the DST shaper, we establish a free-space propagation of a distance R between the mask and the diffraction grating, as is shown in Fig. 2. Here, the imaging constraint conventionally imposed in the DST shaper with respect to the spatial masking operation has been removed. The result is that the spatial amplitude distribution just prior to the grating $s(x)$ is no longer simply a scaled image of the mask $m(x)$ applied to the input beam; rather, the relation between $s(x)$ and $m(x)$ is a Fresnel transform (this distinction is made visually in Figs. 2 and 3 by representing the physical mask $m(x)$ in gray and the complex spatial amplitude distribution before the grating, $s(x)$, in black). Then, it follows from Eq. (8) that the output temporal field is given by

$$e_{out}(t) \propto e_{in}(t) * m\left(-\frac{\alpha}{\gamma}t\right) * exp\left(-i\frac{\pi}{\lambda_o R}\frac{\alpha^2}{\gamma^2}t^2\right). \tag{11}$$

The dispersion (quadratic phase exponential in Eq. (11)) of the output temporal waveform may then be tuned by changing the longitudinal position of the mask (R). In order to change the sign of the dispersion, a virtual Fresnel pattern of the mask (with $R<0$) should be placed over the grating with the help of a lens system. It should be noted that this behavior is distinctly different than that of the conventional DST pulse shaper. In previous work [8, 11] it was shown that illumination of the mask $m(x)$ with a converging / diverging input beam and / or variation

#8348 - $15.00 USD Received 4 August 2005; revised 20 September 2005; accepted 21 September 2005

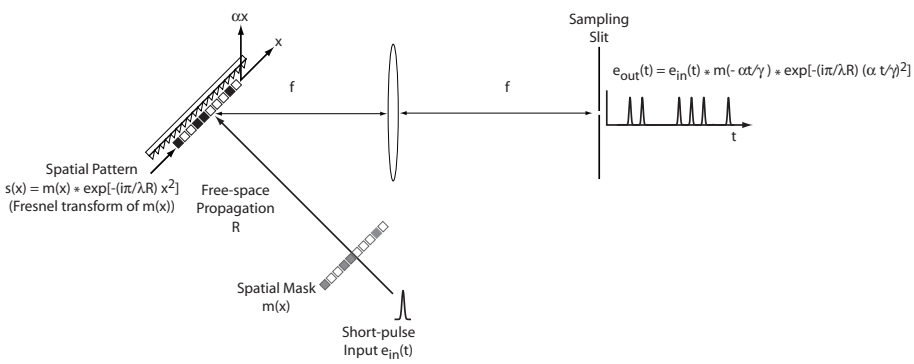

Fig. 2. Schematic representation of the DST pulse-shaper with controlled output dispersion. In contrast to the conventional DST pulse shaper, the spatial amplitude distribution $s(x)$ is not necessarily related to the mask $m(x)$ by a simple projection operation due to the free space propagation through the distance R. Thus, the spatial amplitude distribution at the grating is now the (tunable, based on the distance R) Fresnel transform of the mask.

in the pulse shaping lens position after the grating, results in a multiplicative quadratic spatial phase. After space-to-time conversion in the apparatus, the result is a time-domain waveform that exhibits a quadratic temporal phase, or chirp. Here, free space propagation of the masked optical field prior to the diffraction grating yields the convolution of the mask with a quadratic spatial phase as expressed in Eq. (10). Thus, after space-to-time conversion, the time-domain output of our apparatus exhibits a quadratic spectral phase, or dispersion in the time-domain.

In general, one would have to compute the above convolution to determine the shape of the output temporal waveform; however, in the limits of either a very small, or very large, distance R the output of the pulse shaper may be simply determined. It can be shown [22], that the spatial amplitude distribution applied to the grating $s(x)$ may be variably tuned from the image of the mask $m(x)$ to the spatial FT of $m(x)$ by proper choice of the distance R. The magnitude of the quadratic phase in Eq. (11) determines this relation. For $|R| \ll \pi a^2/\lambda_o$ (where a is the maximum radial extent of the mask) the exponential tends to a spatial delta function and $s(x) \rightarrow m(x)$. The temporal output of the pulse shaper in this case is a scaled version of the input mask as expected in the DST pulse shaper. When the distance R is large enough to consider that the grating is localized in the Fraunhofer region of the mask ($|R| \gg \pi a^2/\lambda_o$), the spatial amplitude distribution immediately before the grating is given by

$$s(x) = M\left(\frac{2\pi}{\lambda_o R}x\right) exp\left(-i\frac{\pi}{\lambda_o R}x^2\right). \tag{12}$$

Then, the temporal output of the shaper is the convolution of the input pulse with the product of the Fourier transform of the input mask (M) and a quadratic temporal phase exponential (frequency modulation).

$$e_{out}(t) \propto e_{in}(t) * \left[M\left(-\frac{2\pi}{\lambda_o}\frac{\alpha}{R\gamma}t\right) exp\left(-i\frac{\pi}{\lambda_o R}\frac{\alpha^2}{\gamma^2}t^2\right)\right], \tag{13}$$

2.3. *Dispersion control in the compact reprogrammable DST pulse shaper*

The architecture of the compact reprogrammable DST pulse shaper is shown in Figure 3. The first element is a 128-pixel, dual-layer liquid crystal spatial light modulator. Since dual-layer

#8348 - $15.00 USD Received 4 August 2005; revised 20 September 2005; accepted 21 September 2005

LC-SLMs allow independent control of both the amplitude and phase of the incoming beam, we are able to simultaneously implement the desired mask $m(x)$ and a quadratic spatial phase corresponding to a converging lens in the SLM device. After free-space propagation through a distance R, the tailored beam impinges on a diffraction grating. In contrast to the conventional DST, the new position of the lens (superposed with the mask) allows a reduction of the total size of the setup by a factor of two. Moreover, the inclusion of the programmable SLM enables dynamic control of both the mask $m(x)$ as well as the focal length of the pulse shaper lens. To develop a theoretical understanding of our system, we calculate the complex spatial amplitude distribution $s(x)$ just prior to the diffraction grating. A simple and effective method to accomplish this is through the Fresnel diffraction integral expressed in terms of the ABCD matrix formalism [21]. From the mask $m(x)$ (implemented in the SLM) to the grating, the system is described by two matrices: one corresponds to the lens of focal length f (also implemented by the SLM) and the other to free-space propagation through a distance R,

$$\begin{aligned}\begin{bmatrix} A & B \\ C & D \end{bmatrix} &= \begin{bmatrix} 1 & R \\ 0 & 1 \end{bmatrix}\begin{bmatrix} 1 & 0 \\ -1/f & 1 \end{bmatrix} \\ &= \begin{bmatrix} 1 & 0 \\ -1/f_{eq} & 1 \end{bmatrix}\begin{bmatrix} M_{eq} & 0 \\ 0 & 1/M_{eq} \end{bmatrix}\begin{bmatrix} 1 & L_{eq} \\ 0 & 1 \end{bmatrix}.\end{aligned} \tag{14}$$

For simplifying the analysis of this optical system, it is worth noting that any *ABCD* matrix can be decomposed into simpler matrices of easier interpretation. In general, an *ABCD* system can be expressed as the concatenation of three simple cascaded elements: a free-space propagation thought the equivalent distance $L_{eq} = B/A$, a scaling factor $M_{eq} = A$, and a lens of equivalent focal length, $f_{eq} = -A/C$ [23, 24]. In this particular configuration,

$$L_{eq} = \frac{Rf}{f-R}, \tag{15}$$

$$M_{eq} = \frac{f-R}{f}, \tag{16}$$

$$f_{eq} = f-R. \tag{17}$$

With these definitions, the equivalent optical system defined by free space propagation through a distance L_{eq}, magnification by M_{eq}, followed by a lens of focal length f_{eq} (as in Eq. (14)) provides the complex spatial amplitude distribution $s(x)$ immediately before the grating. Note, this equivalent system provides a more intuitive view of the functionality of our apparatus. The Fresnel diffraction integral resulting from this equivalent system yields the following field distribution immediately prior to the grating,

$$E_g^-(x,\omega) = E_{in}(\omega)\, s(x) = \left\{ m\left(\frac{x}{M_{eq}}\right) * exp\left(-i\frac{\pi}{\lambda_o L_{eq}}\frac{x^2}{M_{eq}^2}\right)\right\} exp\left(i\frac{\pi}{\lambda_o f_{eq}}x^2\right), \tag{18}$$

where $E_{in}(\omega)$ is the input optical spectrum.

The effect of the diffraction grating is again to impart a spatial scaling (α) and linear spatial phase to the incident field. As a result, the field immediately after the diffraction grating is given by

$$\begin{aligned}E_g^+(x,\omega) = E_{in}(\omega) &\left\{ m\left(\frac{\alpha x}{M_{eq}}\right) * exp\left(-i\frac{\pi}{\lambda_o L_{eq}}\frac{\alpha^2 x^2}{M_{eq}^2}\right)\right\} \\ &\times exp\left(i\frac{\pi\alpha^2}{\lambda_o f_{eq}}x^2\right) exp\left[-j\gamma(\omega-\omega_o)x\right].\end{aligned} \tag{19}$$

#8348 - $15.00 USD Received 4 August 2005; revised 20 September 2005; accepted 21 September 2005

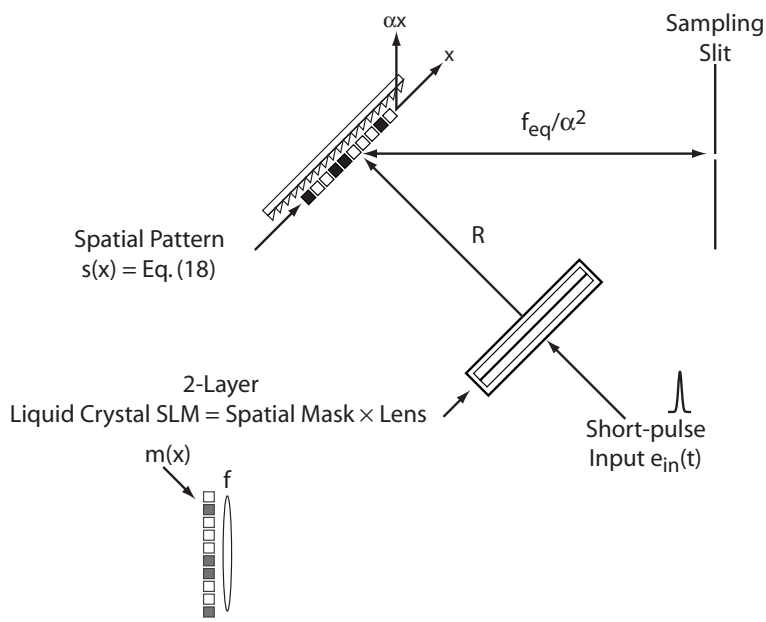

Fig. 3. The compact DST pulse shaper. Here, the LC-SLM allows dynamic reprogramming of both the spatial mask $m(x)$ and the focal length of the pulse shaping lens f.

The quadratic spatial phase due to the lens and change in beam size introduced by the diffraction grating (astigmatism α, Eq. (4)) cause the dispersed optical frequency components to focus at a distance of f_{eq}/α^2 from the diffraction grating. When the sampling slit is placed at this distance, the quadratic spatial phase arising from the pulse shaping lens exactly cancels that arising from propagation through the distance f_{eq}/α^2; thus we again obtain a Fourier transform relation between the field immediately prior to the diffraction grating (Eq. (18)) and the field immediately before the slit. Disregarding a constant phase factor, the field just before the slit is expressed as

$$E_s^-(x,\omega) = E_{in}(\omega)\,\mathscr{F}\left\{ m\left(\frac{\alpha}{M_{eq}}x\right) * exp\left(-i\frac{\pi}{\lambda_o L_{eq}}\frac{\alpha^2}{M_{eq}^2}x^2\right)\right\}, \tag{20}$$

where $\mathscr{F}\{\}$ denotes the spatial Fourier transform evaluated at the spatial frequency k given by

$$k = 2\pi\frac{\alpha^2}{f_{eq}\lambda_o}x - \gamma(\omega-\omega_o). \tag{21}$$

Note, the coupling between optical and spatial frequencies resulting from the diffraction grating (angular dispersion parameter, γ given in Eq. (3)) is included in k. Finally, in order to obtain the time-domain output of our system we again sample the field of Eq. (20) with an ideal spatial delta function slit (as described in section 2.1) and perform an inverse Fourier transform of the output spectrum with respect to optical frequency. The resulting temporal output is given by

$$e_{out}(t) \propto e_{in}(t) * m\left(-\frac{\alpha}{\gamma'}t\right) * exp\left(-i\frac{\Phi_2}{2}\frac{\alpha^2}{\gamma'^2}t^2\right). \tag{22}$$

Here the output temporal waveform is given by the convolution of the input pulse $e_{in}(t)$ with a scaled version of the applied mask $m(x)$ and a quadratic phase factor. In Eq. (22), γ'/α is the

#8348 - $15.00 USD Received 4 August 2005; revised 20 September 2005; accepted 21 September 2005

scaled space-to-time conversion constant and Φ_2 is the dispersion arising from the lens of focal length f (implemented by the SLM) followed by free-space propagation R - this is equivalent to propagation through a distance L_{eq} as expressed in Eq. (15)

$$\frac{\gamma'}{\alpha} = M_{eq}\frac{\gamma}{\alpha}, \tag{23}$$

$$\Phi_2 = \frac{2\pi}{\lambda_o}\frac{1}{L_{eq}}. \tag{24}$$

By properly selecting the parameters of the system (R and f) it is possible to control the dispersion and magnification of the pulse by tuning Φ_2 and γ'/α. These results increase the versatility of the previous DST pulse shaper in the $f-f$ configuration by allowing the relation between the user-defined mask $m(x)$ and output temporal waveform $e_out(t)$ to variably tuned. The relation between these two quantities may be a direct scaling, Fourier transform, or Fresnel transform and is determined by the parameters γ' and Φ_2. In the specific situation when $R = 0$, Eq. (22) reduces to Eq. (8) and the system functions as a conventional DST shaper, though exhibits a 2x shorter footprint.

3. Experimental Results

3.1. Experimental verification in the time domain

We now present several experimental examples of the functionality of the compact reprogrammable DST pulse shaper. In our experiments the input source is a Ti:Sapphire laser producing $\sim$100 fs pulses at a center wavelength around 800 nm. Prior to the shaper, the $\sim$2mm diameter input beam is expanded transversely by a 5.5x cylindrical telescope and, for the 600 l/mm diffraction grating, we choose normal incidence.

We first demonstrate the novel Fresnel transform operation of our apparatus which implies the presence of the quadratic phase term Φ_2 in the output pulse. To this end, we show that the temporal profile of the output waveform of the pulse shaper has the shape of a specific Fresnel diffraction pattern. In the diffractive optics community, it is well accepted that, in irradiance, the free-space propagation through an *ABCD* system can be fully characterized by the collimated Fresnel number, N_C, and the equivalent magnification M_{eq}, [21]. The collimated Fresnel number is defined by $N_C = a^2/(\lambda_o L_{eq}) = a^2\Phi_2/2\pi$ where a is the maximum radial extent of the input mask. To demonstrate the presence of a Fresnel-like pulse in the output of our DST we selected different values of the N_C for the system. Obviously, a change in N_C causes a change in the spatial profile that impinges on the diffraction grating and, consequently, in the temporal modulation of the shaped pulse. For the case of a spatial mask consisting of a rectangular aperture, the number of ripples in the near-field intensity profile corresponds to the value of N_C and for N_C=0.5 which is roughly the boundary region between near and far fields, the spatial beam has essentially only one smooth central lobe [21].

In the experiments, a thin rectangular aperture was programmed as a mask in the SLM together with a lens of focal distance f = 1.3 m. The size of the aperture was chosen to be $2a$=0.8, 2.4 and 4.8 mm and the distance between the SLM and the diffraction grating was R = 310 mm. This corresponds to N_C = 0.5, 4.4 and 17.7, respectively. The dashed lines in Fig. 4 provide the simulated Fresnel pattern irradiance over the diffraction grating calculated by means of Eq. (18). In the simulation the waist of the Gaussian beam was w_o = 4.1 mm, in consonance with the experimental data. The number of ripples obtained in the simulation are in agreement with the value correspondent to N_C. In the case of N_C = 17.7 ($2a$ = 4.8 mm), the high frequency ripples are not observable due to the pulsewidth of the reference pulse in the cross-correlator. The solid lines of Fig. 4 show the measured intensity cross-correlation of the pulse shaper output with a

#8348 - $15.00 USD Received 4 August 2005; revised 20 September 2005; accepted 21 September 2005

$\sim$100 fs reference pulse directly from the source laser. Taking into account that the theoretical space-to-time conversion constant for the Fresnel pattern is $\gamma/\alpha = \sim$1.67 ps/mm, there is a good agreement between the theoretical and experimental results. The slight mismatch between theory and experiment is likely due to constraints in the system, e.g. the finite-durations of both the input pulse and the reference pulse in the cross-correlator.

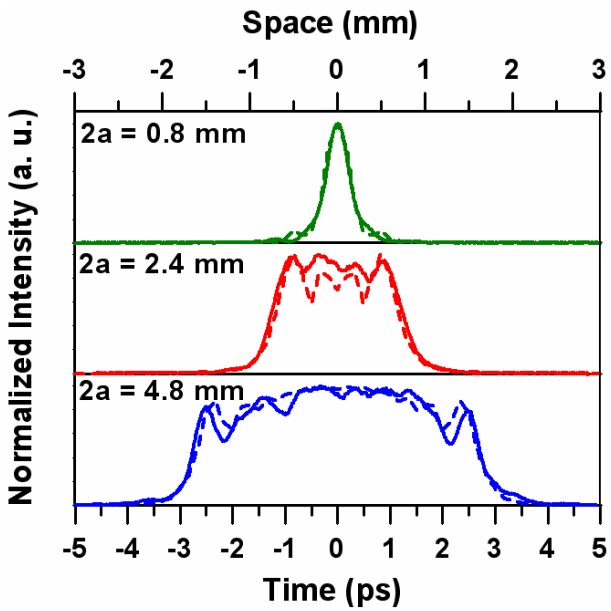

Fig. 4. The solid lines are the measured intensity cross-correlations (bottom axis) of the DST pulse shaper output for a spatial mask $m(x)$ consisting of a slit of width $2a$=0.8 mm (in green), 2.4 mm (in red) and 4.8 mm (in blue) and a lens of focal distance f=1.3 m. The SLM is positioned at a distance R=310 mm from the diffraction grating. The dashed lines show the computer simulations of the Fresnel diffraction pattern over the grating (top axis).

Next, we illustrate the control of the output temporal magnification by manipulation of the equivalent magnification M_{eq} (Eq. 16). We introduce as a mask a multiple aperture in the SLM. The mask is constituted by seven slits each one of width of $2a$ = 0.6 mm and separated by a center-to-center distance of b = 1.0 mm. Mathematically, the multiple aperture can be expressed as

$$m(x) \;=\; rect\left(\frac{x}{2a}\right) * \sum_{n=1}^{7} \delta\left(x - nb\right) \tag{25}$$

After substituting the mask defined by Eq. (25) into the expression for the pulse shaper temporal output given in Eq. (22), in the time domain we expect a pulse sequence given by

$$e_{out}(t) \propto e_{in}(t) * \left[rect\left(-\frac{\alpha}{2a\gamma'}t\right) * exp\left(-i\frac{\Phi_2}{2}\frac{\alpha^2}{\gamma'^2}t^2\right)\right] * \sum_{n=1}^{7} \delta\left[-\frac{\alpha}{\gamma'}\left(t + n\frac{\gamma'}{\alpha}b\right)\right]. \tag{26}$$

This means that the shape of each individual pulse is governed by the convolution of the rect function with the dispersion factor Φ_2 and the global change of the duration of the train of pulses is due to the different values of the space to time conversion constant γ'/α (magnification).

To experimentally observe the change in γ'/α, we modified the focal distance implemented in the SLM to be f = 0.8, 1.0 and 1.3 m. These values correspond to a space-to-time conver-

#8348 - $15.00 USD Received 4 August 2005; revised 20 September 2005; accepted 21 September 2005

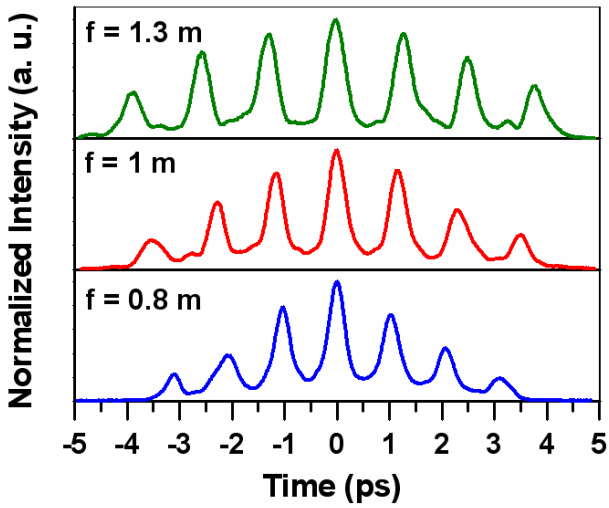

Fig. 5. Intensity cross-correlation measurements of the output pulse sequence of the system of Fig. 3. In the setup the distance R (from the SLM to the diffraction grating in Fig. 3) is fixed to R=310 mm and the focal distance takes the values f=0.8 (blue), 1.0 (red) and 1.3 m (green). The mask is a multiple aperture constituted with seven slits of width 2a=0.6mm and spatial period of 1.0 mm.

sion constant of γ'/α = 0.98, 1.1 and 1.22 ps/mm, respectively. Figure 5 shows experimental intensity cross-correlations obtained for the mask defined by Eq. (25). Notice that an increase in the value of the focal distance causes an increase in the total duration of our wave packet (through the scaled space to time conversion constant γ'/α in Eq. (23) and magnification M_{eq} in Eq. (16)).

3.2. *Scale-tunability in the Fourier passband function of the generalized spectrometer*

Recently, the conventional DST pulse shaper has been demonstrated as a generalized spectrometer with a tunable passband function [18]. In a manner similar to that of Ref. [18], the passband of the spectrometer of Fig. 3 can be tuned from an exact Fourier transform of the mask to a directly scaled version of the mask by simply changing the focal distance implemented in the SLM, the position of the output slit, or both. Moreover, our configuration offers the new capability of scaling the passband function in the Fourier transformation regime by changing the relative position between the diffraction grating and the focus plane. This can be demonstrated by considering Eq. (20). After sampling the DST shaper output spectrum (Eq. (20)) with an ideal delta-function slit positioned at transverse position x_s, the output power spectrum is given by

$$|E_{out}(\omega)|^2 = \left| E_{in}(\omega) M \left\{ \frac{\gamma'}{\alpha} [\omega - \omega(x_s)] \right\} \right|^2 \tag{27}$$

or alternatively in terms of the wavelength as,

$$|E_{out}(\lambda)|^2 \propto \left| E_{in}(\lambda)\, M \left[\frac{2\pi}{\lambda_o} \frac{f-R}{f} \frac{\lambda(x_s) - \lambda}{p\cos\theta_i} \right] \right|^2 . \tag{28}$$

Notice that the factor $(f-R)/f$ inside the FT of the mask, which allow a modification of the scale of the passband function, is specific to our configuration. It would be equal to 1 when

#8348 - $15.00 USD Received 4 August 2005; revised 20 September 2005; accepted 21 September 2005

$R = 0$ or for the conventional $f - f$ spectrometer.

For the practical implementation of the setup, the distance R was fixed to be R = 310 mm and the focal distances programmed in the SLM were changed to f = 0.8, 1.0, and 1.3 m, respectively. As the input spatial mask, we programmed a periodic binary amplitude sequence in the SLM. The period of this sequence was 0.8 mm and the width of each rectangular aperture was 0.2 mm. As the Fourier transform of a periodic binary amplitude sequence consists of a series of a regularly-spaced diffraction orders, the passband spectrum of our configuration will have a discrete number of wavelengths.

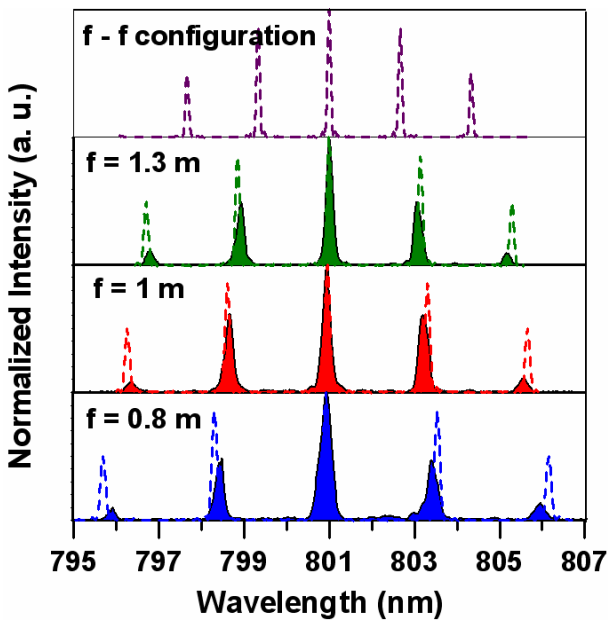

Fig. 6. Spectral scaling properties of the spectrometer with a periodic binary amplitude sequence as an input mask. In the setup the distance R (from the SLM to the diffraction grating in Fig. 3) is fixed to R=310 mm and the focal distance is varied from f=0.8 (blue), 1.0 (red), to 1.3 m (green). The dashed lines indicate the simulated position of the peaks for a flat spectrum. The top trace illustrates the spectrum that should be obtained in the conventional case of $f - f$ alignment.

Experimental results that validate Eq. (28) are show in Fig. 6. Dashed lines show the computer simulations assuming a rectangular input optical spectrum, i.e. $E_{in}(\lambda) = 1$ over the spectrum of the pulse. As expected the passband function of the spectrometer consists of peaks with different weight. In reality, the spectrum of the input pulse is approximately sech or Gaussian function. Then, the simulation indicates the position of the peaks but gives no information about its spectral intensity which should decay more strongly for wavelengths far away from the center wavelength of 801 mm. The experimental results, in agreement with the simulations, are shown by the solid lines. The top trace shows the predicted output spectrum for a conventionally-aligned $f - f$ spectrometer with the same input spatial mask (a binary amplitude sequence). If we focus our attention on the maximum of the peak in the spectrum that corresponds to the third order of diffraction of the binary amplitude mask, its transverse position moves from $\sim$805.15 nm to $\sim$806 nm as the spectrometer focal length is varied. This example clearly illustrates how the scale of the Fourier passband function of the spectrometer

#8348 - $15.00 USD Received 4 August 2005; revised 20 September 2005; accepted 21 September 2005

may be varied by modifying the parameters of the system.

4. Conclusion

In conclusion, we present a novel programmable Fresnel transformer pulse shaper which increases the flexibility of the conventional DST pulse shaper. In the conventional DST pulse shaper, the mask (or its image) is located at the diffraction grating. Here, we modified this device by introducing a free-space propagation between the mask and the grating and by constructing a shorter configuration based on a converging input beam. These changes allow the spatial convolution associated with free-space propagation to be translated into dispersion of the temporal output of the pulse shaper. Then, by changing the parameters of the system, we demonstrate control of this dispersion as well as the space-to-time conversion constant in the pulse shaping apparatus (magnification of the output waveform). In addition, to increase the versatility of the Fresnel transformer pulse shaper and to attain dynamic control of the setup, we implement the mask and the pulse shaping lens in a programmable dual-layer liquid-crystal spatial light modulator. This allows computer control over both the spatial mask applied in the pulse shaper, as well as the dispersion and magnification of the temporal output, on the millisecond timescale. In addition to new temporal behavior, we also demonstrate - theoretically and experimentally - that the passband function determined by the Fourier transform of the mask, can be obtained with a user-defined scaling factor.

This work was performed in the Ultrafast Optics and Fiber Communications Laboratory at Purdue University (USA). G. Mínguez-Vega gratefully acknowledges the friendship of the members of this group and the financial support from the Fundació Caixa Castelló-Bancaixa and the Conselleria de Cultura, Educació i Esport (GV04B-018).